**Iğdır Üniversitesi Fen Bilimleri Enstitüsü Dergisi, 15(4), 1311-1328, 2025**
***Journal of the Institute of Science and Technology, 15(4), 1311-1328, 2025***

**ISSN: 2146-0574, eISSN: 2536-4618**

**Elektrik Elektronik Mühendisliği / *Electrical Electronic Engineering*** **DOI: 10.21597/jist.1651197**

**Araştırma Makalesi / *Research Article***

**Geliş tarihi / *Received*: 04.03.2025** **Kabul tarihi / *Accepted*: 26.05.2025**

**Atıf İçin:** Alpsalaz, F. & Türkay, Y. (2025). Seri hibrit elektrikli araçta süperkapasitör & lityum iyon batarya yönetimi. *Iğdır Üniversitesi Fen Bilimleri Enstitüsü Dergisi*, 15(4), 1311-1328.

***To Cite:*** Alpsalaz, F. & Türkay, Y. (2025). Supercapacitor and lithium-ion battery management in a series hybrid electric vehicle. *Journal of the Institute of Science and Technology*, 15(4), 1311-1328.

# Seri Hibrit Elektrikli Araçlarda Süperkapasitör & Lityum İyon Batarya Yönetimi

Feyyaz ALPSALAZ[1*], Yavuz TÜRKAY[2]

**Öne Çıkanlar:**

- Süperkapasitörler & lityum-iyon bataryalar entegre edilerek enerji verimliliği & performans artırılmıştır.
- Batarya Yönetim Sistemi geliştirilmiştir.
- Sürüş Çevrimleri Uygulanmıştır

**Anahtar Kelimeler:**

- Enerji yönetim sistemi
- Hibrit elektrikli araç
- Lityum-iyon batarya
- Süperkapasitör

**ÖZET:**

Bu çalışma, lityum-iyon (Li-ion) bataryalar & süperkapasitörler (SC) ile donatılmış bir seri hibrit elektrikli araç (SHEV) için gelişmiş bir enerji yönetim sistemi (EMS) önermektedir. Geliştirilen kural tabanlı EMS, içten yanmalı motor (ICE), elektrik motoru (EM) & enerji depolama sistemi (ESS) arasındaki güç dağıtımını optimize ederek enerji kullanımını verimli hale getirirken batarya ömrünü & araç performansını artırmaktadır. Önerilen EMS, gerçek zamanlı sürüş koşulları & şarj durumu temelinde güç akışını dinamik olarak ayarlayarak aşırı şarj/deşarj akımlarını önlemekte & rejeneratif frenleme verimliliğini artırmaktadır. Araç performansını değerlendirmek için Gelişmiş Araç Simülatörü platformu (ADVISOR) kullanılarak Kentsel Dinamometre Sürüş Çevrimi (UDDS) & Yeni Avrupa Sürüş Çevrimi (NEDC) koşullarında kapsamlı bir simülasyon gerçekleştirilmiştir. Elde edilen sonuçlar, EMS'nin enerji verimliliğini önemli ölçüde artırdığını, yakıt tüketimini azalttığını & batarya ömrünü uzattığını göstermektedir. Karşılaştırmalı analiz, NEDC sürüş çevriminde daha dengeli hızlanma & frenleme desenleri nedeniyle daha üstün bir performans sergilendiğini ortaya koymuştur. Bu bulgular, süperkapasitörlerin Li-ion bataryalar ile entegrasyonunun SHEV mimarilerinde etkin bir çözüm sunduğunu & sürdürülebilir, verimli hibrit araç tasarımı için önemli bir katkı sağladığını göstermektedir.

# Supercapacitor and lithium-ion battery management in a series hybrid electric vehicle

**Highlights:**

- Supercapacitors and lithium-ion batteries are integrated for enhanced energy efficiency and performance.
- A Battery Management System has been developed.
- Driving Cycles have been implemented.

**Keywords:**

- Hybrid electric vehicle
- Energy management system
- Lithium-ion battery
- Supercapacitor

**ABSTRACT:**

This study proposes an advanced EMS for a SHEV equipped with lithium-ion (Li-ion) batteries and supercapacitors (SC). The developed rule-based EMS optimizes power distribution between the internal combustion engine (ICE), electric motor (EM), and energy storage system (ESS), ensuring efficient energy utilization while enhancing battery lifespan and vehicle performance. The proposed EMS dynamically adjusts power flow based on real-time driving conditions and charge state, preventing excessive charge/discharge currents and improving regenerative braking efficiency. A comprehensive simulation was conducted using the ADVISOR (Advanced Vehicle Simulator) platform to evaluate vehicle performance under Urban Dynamometer Driving Schedule (UDDS) and New European Driving Cycle (NEDC) conditions. Results demonstrate that the EMS significantly enhances energy efficiency, reduces fuel consumption, and extends battery longevity while ensuring optimal power delivery. Comparative analysis reveals superior performance under NEDC conditions due to smoother acceleration and braking patterns. These findings highlight the effectiveness of integrating supercapacitors with Li-ion batteries in SHEV architectures, providing a viable solution for sustainable and efficient hybrid vehicle design.

[1*]Feyyaz ALPSALAZ (**Orcid ID:** 0000-0002-7695-6426 ), Yozgat Bozok University, Akdağmadeni Vocational School, Department of Electricity and Energy, Yozgat, Türkiye
[2]Yavuz TÜRKAY (**Orcid ID:** 0000-0002-4263-8286 ), Sivas Cumhuriyet University, Faculty of Engineering, Department of Electrical and Electronics Engineering, Sivas, Türkiye

***Sorumlu Yazar/*Corresponding Author**:** Feyyaz ALPSALAZ, e-mail: feyyaz.alpsalaz@bozok.edu.tr

This study was produced from Feyyaz ALPSALAZ's Master's thesis.

## INTRODUCTION

The total number of vehicles in the world is increasing exponentially. Due to the exponentially increasing number of vehicles, exhaust emissions are also increasing exponentially. Vehicle exhaust emissions are considered as one of the reasons of global warming. According to the Intergovernmental Panel on Climate Change (IPCC) report, fossil fuels (oil, natural gas and coal) account for 86% of global emissions in the last decade (Foyer et al., 2018; Jackson et al., 2019).

Vehicle exhaust emissions account for 45% of the hydrocarbon ($C_nH_{2n+2}$) released into the atmosphere, 55% of nitrogen oxide (NO) and 65% of carbon monoxide (CO). The most important reason for turning to electric vehicles recently is to reduce exhaust emissions. (Kerem, 2014). Although it is not known who first invented the electric vehicle, many inventors succeeded in producing electric vehicles with various features in the 1830s. The first commercially viable electric car was built by Thomas Parker in London in 1879. However, in the early 1900s, the demand for electric vehicles decreased due to the low cost and extended driving range of internal combustion engine (ICE) vehicles. It is a known fact that the costs of electric vehicles are still higher than internal combustion engine vehicles. Until the 1970s, electric vehicles were less preferred than ICE-powered vehicles due to their low energy density battery and cost. (K. Chau et al., 1999). Due to the increase in oil prices in parallel with the great oil crisis that broke out in the 1970s, the trend towards electric vehicles has increased in order to reduce oil dependence and exhaust emissions. (Baur & Todorova, 2018; Costa et al., 2021; Soylu & Soylu, 2011). Energy storage systems (ESS), one of the most important components of electric vehicles, are required to operate in optimum conditions. (Chau and Wong, 2002) The choice of technology to be used in energy storage systems is selected based on cycle life, efficiency, power density and energy density criteria (Mi and Masrur, 2017). Multiple storage elements are used because of their high efficiency and longer range in ESSs (Khaligh and Li, 2010; Mitkowski and Skruch, 2013). In the case of multiple ESSs used together, the biggest problem is optimization (Jinrui et al., 2006). Energy optimization is required to obtain the required efficiency and better performance from the batteries, electric motor and regenerative reverse braking energy (Pérez et al., 2006).

When the studies in the literature are examined, low-level and high-controller algorithms have been proposed by applying the optimization-based optimal predictive control strategy against the optimization problems of EMS in electric vehicles (Tie and Tan, 2013). Thus, the advantages and disadvantages of the optimization strategy according to driving cycles were investigated (Michalczuk et al., 2013). Trovão et.al (2013), a rule-based meta-heuristic optimization strategy integrated with a multi-level energy management system was used for energy and power sharing between two sources with different characteristics, a supercapacitor and a battery. In addition to the previously known driving cycles, it has also been independently considered online(Trovão et al., 2013). Ferreira et.al (2008), an energy management strategy based on fuzzy logic optimization has been revealed for two energy storage devices (lead-acid batteries and supercapacitors). The Control strategy is purposed to ensure efficient operation of the individual power supply by regulating the voltage to provide the desired power. In another study (Liu and Liu, 2022), an energy management system was proposed with a rules-based feedback control algorithm strategy in electric vehicles. The proposed EMS was compared in terms of vehicle speed and load power by using driving cycles to achieve maximum efficiency in light electric vehicles in case of having more than one energy source(Liu and Liu, 2022). In a different study of a hybrid electric vehicle (He et al., 2012), model predictive control (MPC), the equivalent consumption minimization strategy (ECMS), and dynamic programming (DP) approaches

were compared with optimization methods. The simulation results were found to provide competitive performance for different charge status intervals and driving cycle conditions with a lower calculation load compared to the alternative methods.

Herath et al. (2019) conducted a comparative analysis of optimization-based and rule-based energy management systems (EMS) for a domestic photovoltaic (PV)-battery installation, incorporating time-varying local state of charge (SOC) limits. The study demonstrated that the rule-based EMS achieved equivalent cost optimization results to the mixed integer linear programming (MILP) approach, with significantly lower computational time (approximately 3% of MILP). Additionally, the introduction of local SOC limits enhanced economic performance by reducing reliance on costly utility power during peak perio Herath et al. (2019) conducted a comparative analysis of optimization-based and rule-based energy management systems (EMS) for a domestic photovoltaic (PV)-battery installation, incorporating time-varying local SOC limits. The study demonstrated that the rule-based EMS achieved equivalent cost optimization results to the mixed integer linear programming (MILP) approach, with significantly lower computational time (approximately 3% of MILP). Additionally, the introduction of local SOC limits enhanced economic performance by reducing reliance on costly utility power during peak periods, particularly under deviations from predicted load and PV generation profiles (Herath et al., 2019).ds, particularly under deviations from predicted load and PV generation profiles (Herath et al., 2019). Domarchi and Cherchi (2023) conducted a critical review of EV demand forecasting models, focusing on the integration of choice behavior and diffusion processes. Unlike prior reviews, it specifically examines how fuel type choice is incorporated into diffusion models, assesses forecast accuracy using root mean square error (RMSE) against actual market data, and compares model strengths and limitations. Analyzing 54 articles from 2008–2021, the study categorizes models into bottom-up (e.g., agent-based models), top-down (e.g., system dynamics), and mixed approaches. Findings show mixed models achieve the highest accuracy, with pessimistic scenarios best matching actual EV adoption rates, highlighting the importance of robust data and calibration for reliable predictions (Domarchi & Cherchi, 2023).

Although previous studies have proposed rule-based EMS strategies for HEVs, they have often focused on a single energy storage system or failed to dynamically adapt to real-time driving conditions. This paper presents an innovative rule-based EMS that synergistically integrates supercapacitors and lithium-ion batteries in SHEVs. Unlike existing approaches, our proposed EMS dynamically adjusts power distribution based on real-time driving cycles and SOC to evenly distribute energy efficiency, extend battery life, and improve regenerative braking performance. This addresses critical gaps in providing balanced power management in different urban and highway driving conditions. In this study, a new EMS based on the rule-based control strategy of supercapacitors and lithium-ion batteries has been proposed. The control strategy is constructed to achieve maximum efficiency from batteries and electric motors and to compensate for sudden drops in discharge currents of batteries. While conventional rule-based EMS strategies are typically based on static thresholds, our proposed approach dynamically adjusts power output according to SOC, vehicle speed and torque demand in real time. This enables efficient use of supercapacitors for high-torque scenarios, while accurately distributing the continuous power supply from lithium-ion batteries, reducing battery stress and improving overall system efficiency.

## MATERIALS AND METHODS

In this section, energy storage systems, an internal combustion engine model, an electric motor model, DC / DC converter, vehicle dynamics and drivetrain subsystems are modeled analytically

## Energy Storage Systems

In this study, the selection of energy storage resources is made according to Table 1. Lithium-ion batteries have high cycle life and high-power density. The required power in the electric vehicle architecture is distributed between the proposed EMS algorithm and the energy storage resources.

**Table 1.** Energy storage components used in HEV

| Storage | Cycle Life | Efficiency (%) | Power Density (W/kg) | Energy Density (Wh/kg) | Ref. |
|---|---|---|---|---|---|
| Lead-acid | 1500-5000 | 80-90 | 180 | 35-40 | (May et al., 2018) |
| Lithium ion | 2000 | >95 | 250-1000 | 100-265 | (Cao et al., 2014) |
| NiMH | >3000 | 75 | 250-1000 | 60-120 | (Young, 2016) |
| Super-capacitor | >500000 | 85-98 | 500-10000 | 1-10 | (Patel et al., 2021) |

The table compares energy storage components used in HEVs. Lead-acid batteries have a cycle life of 1500-5000, an efficiency of 80-90%, a power density of 180 W/kg, and an energy density of 35-40 Wh/kg. Lithium-ion batteries offer a cycle life of 2000, efficiency above 95%, power density ranging from 250 to 1000 W/kg, and energy density between 100-265 Wh/kg. Nickel-metal hydride (NiMH) batteries have a cycle life of over 3000, 75% efficiency, a power density of 250-1000 W/kg, and an energy density of 60-120 Wh/kg. Supercapacitors exhibit a cycle life exceeding 500,000, efficiency of 85-98%, power density between 500 and 10,000 W/kg, and an energy density of 1-10 Wh/kg.

The lithium-ion battery pack modeling and the supercapacitor package model, which form the energy storage systems, are modeled in the following sections.

## Supercapacitor model

Supercapacitors, also known as ultracapacitors, are energy storage devices that offer high power density and rapid charge-discharge capabilities, bridging the gap between conventional capacitors and batteries. They store energy through the electrostatic separation of charges at the electrode-electrolyte interface, enabling longer cycle life and faster response times compared to traditional batteries. The equivalent circuit model given in Figure 1 is used as a mathematical model in the simulation architecture. Where $R_s$ is charge/discharge resistance and $R_p$ symbolizes self-discharge losses.

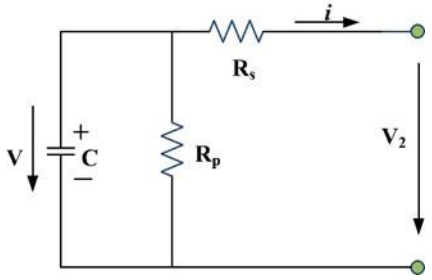


**Figure 1.** Equivalent circuit of the supercapacitor

$$V(t) = V_0 e^{-\frac{t}{\tau}} \quad (1)$$

$$Q = Q_0 - \int_0^t i dt \quad (2)$$

Where, V(t) is the instant voltage for the supercapacitor during discharge, C is supercapacitor capacitance, $V_0$ is initial voltage, $V_2$ is terminal voltage, Q is total charge and $\tau$ is the time constant dependent on C.

The supercapacitor bank is modeled using cascade supercapacitor cells in parallel/series. In this model, The total capacitance and resistance of the super capacitor bank are defined in equations (3) and (4):

$$R_{sc\_bank} = \frac{n_1}{n_2} R_s \quad (3)$$

$$C_{sc\_bank} = \frac{n_1}{n_2} C \quad (4)$$

where $n_1$ represents how many capacitors are in series and $n_2$ represents how many branches are in parallel. If the Ragone test is applied for the supercapacitor , the td discharge and tc charging times are obtained as follows depending on the terminal output power P2 (Zhang and Mi, 2011).

$$t_d = \frac{C[P_2R_s(ln(P_2R_s) - ln(V_{20d}^2)) + V_{20d}^2 - P_2R_s]}{2P_2} \quad (5)$$

$$t_d = \frac{C[P_2R_s(ln(P_2R_s) - ln(V_{20d}^2)) + V_{20d}^2 - P_2R_s]}{2P_2} \quad (6)$$

Where, $V_{20d}$ is the output discharge voltage and $V_{20c}$ is the output charge voltage. The efficiency of the supercapacitor model is obtained as follows:

$$\eta = \frac{t_dP_2}{t_cP_2} = \frac{P_2R_s(ln(P_2R_s) - ln(V_{20d}^2)) + V_{20d}^2 - P_2R_s}{-P_2R_s(ln(P_2R_s) - ln(V_{20c}^2)) + V_{20c}^2 - P_2R} \quad (7)$$

Where, Ed represents the output discharge voltage, $E_c$ is the output charge voltage, $V_{20c}$ is the branch voltage when the electric charge approach $Q_0$, and $V_{20d}$ represents the branch voltage when the electric discharge reaches $Q_0$.

**Li-ion battery model**

Li-ion batteries are rechargeable energy storage devices widely used for their high energy density, lightweight design, and long cycle life. They operate through the movement of lithium ions between the anode and cathode, facilitated by an electrolyte, making them ideal for applications requiring sustained power, such as electric vehicles and portable electronics. The equivalent circuit Rint model of the lithium battery, which is another ESS to be used in simulation architecture, is shown in Figure 2. Where, the open-circuit voltage is symbolized by E, Resistors $R_1$ and $R_2$ make up the two-component internal resistor Rint and C is capacitance that characterizes the transient response of the charge doublet.

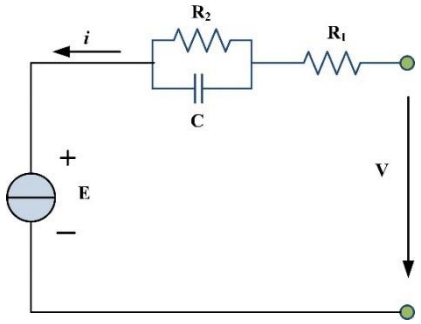


**Figure 2.** Lithium-ion battery equivalent circuit

The potential is obtained by the following equations expressing the relationship between branch voltage and SOD (Gao et al., 2002):

$$E[i(t), T(t), t] = V[i(t), T(t), t] - R_{int} \quad (8)$$

$$V[i(t), T(t), t] = \sum_{k=0}^{n} C_k SOD^k[i(t), T(t), t] + \Delta E(T) \quad (9)$$

$$SOD[i(t), T(t), t] = \frac{1}{C_r} \int_0^t \alpha[i(t)]\, \beta[T(t)] i(t) dt \quad (10)$$

where, the SOD is a state of discharge, the term, $C_k$ is the $k^{th}$ term for the reference curve in the polynomial expression, Cr is the battery capacity, α(i), dependency ratio factor of SOD and β(T)

temperature factor of SOD. The (8), (9) and (10) circuit model variables modeled with the charge and discharge energies are obtained as follows.

$$E_{dis} = \int_0^{t_d} P_c dt = t_d(E - R_{int}) \quad (11)$$

$$E_{chg} = \int_0^{t_d \int} P_c dt = t_d(E + R_{int}) \quad (12)$$

In the above equations, the charge energy is represented by $E_{chg}$ and the discharge energy needed to charge the same rate again as $E_{dis}$. Thus, the efficiency of the lithium-ion battery to be modeled is calculated by the ratio of the discharge energy to the charge energy.

$$\eta_B = \frac{E_{dis}(t)}{E_{chg}(t)} = \frac{E - R_{int}}{E + R_{int}} \quad (13)$$

## Electric Motor Model

The modeling equivalent circuit of the permanent magnet synchronous motor (PMSM) to be used in the electric vehicle architecture is shown in Figure 3. An equivalent circuit model used in mathematical modeling was applied (Karabacak and Eskikurt, 2012).

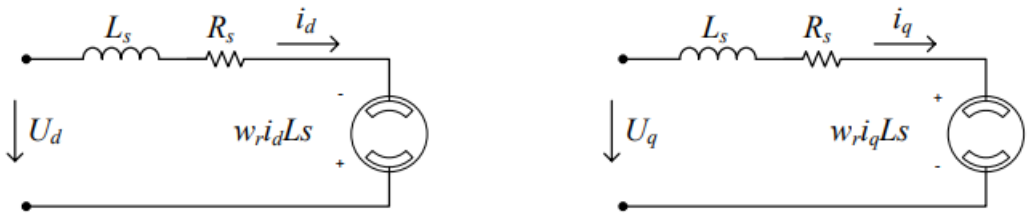


**Figure 3.** Equivalent circuit of the electric motor

$$U_d = \frac{d\Psi_d}{dt} - \Psi_{ds} + R_s i_d \quad (14)$$

$$U_q = \frac{d\Psi_q}{dt} - \Psi_{ds} + R_s i_q \quad (15)$$

where $L_s$ is the stator inductance, Ψ indicates the permanent magnet flux. Due to the permanent magnetic field, the stator current with direct axis can be controlled to reach zero. In other words, if id=0, the electromagnetic torque produced in the rotor is shown as follows:

$$T_e = \frac{3p}{2}\left(i_q \Psi_d - i_d \Psi_q\right) = \frac{3p}{2}\left(i_q \Psi_r\right) \quad (16)$$

$$T_e = J\frac{d\omega_r}{dt} + B_r + T_L \quad (17)$$

The electromagnetic torque is as given in equation (17) in terms of motor dynamic equations. Where, Te represents the torque produced by the motor, $\omega_r$ is the mechanical speed, J is the moment of inertia, B is the coefficient of friction and $T_L$ is the torque of the load. Subtracting $\omega_r$ in equation (18), the following equation is obtained.

## DC/DC Boost Converter

For the DC-DC Boost converter, state space modeling technique is used to analyze it in both time and frequency space. (Tan and Hoo, 2015). The boost converter circuits and its 'ON' / 'OFF' state circuits are shown in Figure 4. When 'ON' state, the inductor is charged via $U_1$ defined in (22). In this case, where the diode is an open circuit as defined in (23), there is no current flow to the capacitor and resistor.

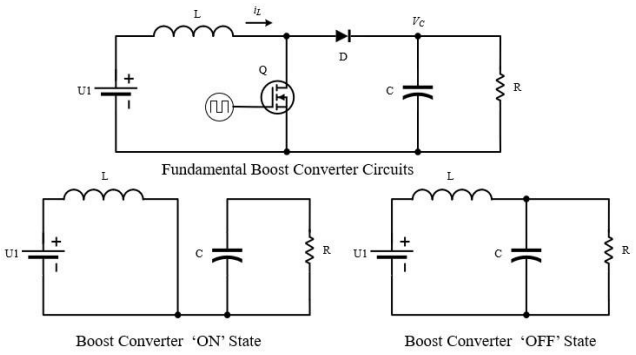


**Figure 4.** DC-DC boost converter

When 'ON' state, the inductor is charged via $U_1$ defined in (19). In Equation (20) it is 'OFF' state of the Diode and in this case, there is no current flow to the capacitor and resistor.

$$U_1 = L\frac{di_L}{dt} \quad (19)$$

$$C\frac{dV_C}{dt} + \frac{V_C}{R} = 0 \quad (20)$$

By rearranging (20) and (21), the $\dot{x}_1$ and $\dot{x}_2$ state derivatives in (21) and (22) are obtained. Using (21) and (22) the state space matrix of the 'ON' boost converter can be formulated as in (23).

$$x_1{}' = \frac{1}{L}u_1 \quad (21)$$

$$x_2{}' = -\frac{x_2}{RC} \quad (22)$$

$$\begin{bmatrix} x_1{}' \\ x_2{}' \end{bmatrix} = \begin{bmatrix} 0 & 0 \\ 0 & \frac{-1}{RC} \end{bmatrix} . \begin{bmatrix} x_1 \\ x_2 \end{bmatrix} + \begin{bmatrix} \frac{1}{L} \\ 0 \end{bmatrix} U_1 \quad (23)$$

The state space matrix 'ON' and 'OFF' state average values of the boost converter can be formulated using the switching duty cycle d. Space matrices mean values (24) and (25) are shown.

$$\bar{A} = \begin{bmatrix} 0 & 0 \\ 0 & -\frac{1}{RC} \end{bmatrix} d + \begin{bmatrix} 0 & -\frac{1}{L} \\ 1 & -\frac{1}{RC} \end{bmatrix} (1-d) = \begin{bmatrix} 0 & -\frac{1-d}{L} \\ \frac{1-d}{C} & -\frac{1}{RC} \end{bmatrix}$$

(24)

$$\bar{B} = \begin{bmatrix} \frac{1}{L} \\ 0 \end{bmatrix} d + \begin{bmatrix} \frac{1}{L} \\ 0 \end{bmatrix} (1-d) = \begin{bmatrix} \frac{1}{L} \\ 0 \end{bmatrix} \quad (25)$$

Where, (24) and (25) represent matrices used in (23) to complete the boost converter model. Equation (26) presents the amplifier converter state-space model in its final form.

$$\begin{bmatrix} x_1{}' \\ x_2{}' \end{bmatrix} = \begin{bmatrix} 0 & -\frac{1-d}{L} \\ \frac{1-d}{C} & -\frac{1}{RC} \end{bmatrix} \begin{bmatrix} x_1 \\ x_2 \end{bmatrix} + \begin{bmatrix} \frac{1}{L} \\ 0 \end{bmatrix} U_1 \quad (26)$$

**Vehicle Dynamics**

In the simulation architecture, the longitudinal vehicle dynamics model is obtained through the forces acting on the vehicle shown in Figure 5. Since only uphill running is taken into account in the vehicle performance analysis, the slope force is written in figure 5 as follows:

$$F_g = M_v g \sin a$$

(27)

Since the vehicle's road angle α is small, the slope can be defined as:

$$\zeta = \frac{H}{L} = tan\ \alpha \cong sin\ \alpha \quad (28)$$

The resistance of the tire rolling resistance $F_f$ and the inclination force $F_g$ of the road is calculated together with the indicated resistance of the road $F_{rd}$.

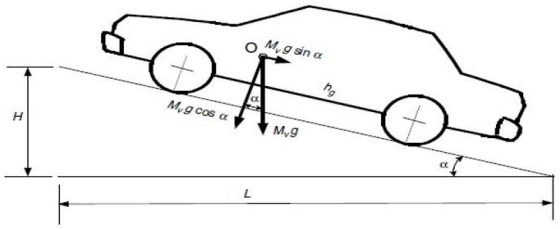


**Figure 5.** The forces acting on the vehicle (Ehsani et al., 2019)

$$F_{rd} = F_f + F_g = M_v g(f_r + \zeta) \quad (29)$$

Where $f_r$ is the rolling resistance and ζ is the slope. If moments of all forces are involved when the vehicle is moving, $W_f$ in the front axle and $W_f$ in the rear axle can be specified as the normal load.

$$W_f = \frac{M_v g L_b cos\alpha}{L} - \frac{T_{rf}+T_{rr}+M_v g h_g sin\alpha+F_\omega h_\omega+M_v h_g\left(\frac{dV}{dt}\right)}{L} \quad (30)$$

$$W_r = \frac{M_v g L_a cos\alpha}{L} + \frac{T_{rf}+T_{rr}+M_v g h_g sin\alpha+F_\omega h_\omega+M_v h_g\left(\frac{dV}{dt}\right)}{L} \quad (31)$$

where $T_{rf}$ and $T_{rr}$ are respectively front and rear rolling resistance moment, $F_w$ aerodynamic friction force, v vehicle speed, $M_v$ vehicle mass, L wheelbase, $h_w$ height of the application center of the aerodynamic resistance, $h_g$ the height of the center of gravity of the vehicle, $L_a$ the distance from the center of gravity of the front wheel, $L_b$ is the distance of the rear wheel from the center of gravity, and g is gravity.

**Internal Combust Engine Model**

ICEs are the component that makes the biggest contribution to the propulsion of hybrid electric vehicles. The operation and speed range of the internal combustion engine will be determined. The thermodynamic efficiency of ICEs operating under steady-state conditions is determined by $\eta_E$, engine speed $\omega_E$, and internal combustion engine torque $T_{ICE}$. The relationship of these parameters is shown by:

$$\eta_E = \frac{\omega_{ICE}.T_{ICE}}{P_k} \quad (32)$$

Here $P_k$, is chemical, which is a sub-symbol because it carries fuel and chemical energy [. The fuel mass flow defined in Equation (34) is the enthalpy current associated with $M_f$. $H_l$ represents a lower heating value of the fuel.

$$M_f = \frac{P_k}{H_l} \quad (33)$$

Average piston velocity $C_m$ defined in equation (35) and average effective pressure $p_m$ defined in equation (36) are normalized engine variables and can represent engine operating point at steady state conditions.

$$C_m = \frac{\omega_{ICE}.S}{\pi} \quad (34)$$

$$p_m = \frac{N.T_{ICE}\pi}{S_d} \quad (35)$$

Where $S_d$ is engine cylinder volume, $p_m$ mean effective presure and S is engine stroke. In equation (36), N = 2 and N = 4 for a two-stroke engine and a four-stroke engine, respectively. The $P_{max}$ value must be known to estimate the motor dimensions. The value of $p_{max}$ is found as follows:

$$P_{max} = \frac{\pi}{16} K\,.\,B^2.p_m.C_m \quad (36)$$

Where K is the number of cylinders and B is the cylinder diameter. As a result, after the nominal motor power $P_{max}$ is determined, it is possible to estimate the motor size associated with the number of cylinders and cylinder bore. For the engine model and dimensions, it is possible to simplify the engine model using the active Willans definition, where the motor approaches the effective pressure value.

$$p_m \approx \eta(\omega_{ICE}).P_f - P_{me}(\omega_{ICE}) \quad (37)$$

In this case, $\eta(\omega_{ICE})$ is the transformation of the thermodynamic energy from the chemical energy to the inside of the cylinder to the pressure inside the cylinder; $P_{me}(\omega_{ICE})$, $\omega_{ICE}$ defines all mechanical friction losses in the motor at the speed of $\omega_{ICE}$ ; and $P_{me}(\omega_{ICE})$ is generally considered a fixed for preliminary calculations. The average fuel pressure of Pf is an average effective pressure at which a motor with 100% efficiency is produced by burning a mass of fuel, pressure is generated by burning a mass of fuel of mf with a 100% yield of a motor and is defined by:

$$P_f = \frac{H_l.m_f}{S_d} \quad (38)$$

In accordance with the experimental data of a 41 kW Geo Metro 1.0 L SI engine to be used in simulation, engine torque, $M_a$ air/fuel mixture ratio depending on the mass of air load A/F, σ spark advancement (top of the center before dead center), and engine speed $\omega_{ICE}$, can be calculated with an empirical relationship as shown below. The motor acceleration state equation is as defined in equation (40).

$$T_{ICE} = -181{,}36 + 379{,}36.M_a + 21{,}91\left(\frac{A}{F}\right) - 0{,}85\left(\frac{A}{F}\right)^2 + 0{,}26\sigma\text{-}0{,}0028.\sigma^2 + 0{,}027.\omega_{ICE} + 0{,}000107.\omega_{ICE}{}^2 + 0{,}00048.\omega_{ICE}.\sigma + 2{,}55.\sigma.M_a - 0{,}5.\sigma^2.M_a \quad (39)$$

$$\frac{d\omega_{ICE}}{dt} = \frac{1}{J_{ICE}}(T_E - T_L) \quad (40)$$

$J_{ICE}$ represents the inertia of the motor torque and $T_L$ the load torque.

**EMS Control Strategy**

A new rule-based EMS has been suggested for a SHEV. For this purpose, in the control study of the vehicle, rules that determine the working areas and working conditions of the EMS and the EMS have been established.

- *Maximum charging level ($SOC_{max}$ )*
- *Minimum charging level ($SOC_{min}$ )*
- *Minimum torque values for the EMS*
- *Charging (torque of the wheel)*
- *Required power and brake zones*

The proposed control strategy in Figure 6 shows the drive or braking condition of the electric vehicle from the wheel torque as a reference.

In the case of vehicle drive (Mwhell>0):

1. If the emission value is smaller than the desired speed value (v <55 km/h) and the charge level is greater than the limit value (SOC> 0.65);

a) If the required torque is smaller than the EM (M < MEm,max), then the drive power is supplied by EM.

b) The requested torque is greater than the EM moment (M > MEm,max), which is only driven by the ICE.

2. If the emission value is less than the desired speed value (v <55 km/h) and the charge level is not sufficient (SOC <0.65),

a) If the requested torque is greater than the minimum moment of (MICE<Mmin), it is supplied by ICE and the battery is charged by the generator.

b) If the required torque is greater than the minimum torque value (MICE>Mmin), the drive is supplied with the ICE.

3. If the vehicle is faster than the specified speed limit (v > 55 km/h),

a) If the charge level is smaller than the specified value and the demanded torque is less than the minimum torque value (MICE<Mmin & SOC<0.8), the generator is activated and the momentum is met by the ICE when the battery is being charged.

b) If the charge level is greater than the specified value or the demanded torque is greater than the minimum torque value (MICE > Mmin & ya SOC>0.8), then the drive is supplied only with the ICE.

If the vehicle is braked (Mwheel <0);

1. If the battery level is below a certain maximum value (SOC <0.9);

a) If the brake torque is less than the EM maximum torque (M<MEM,max), the battery is recharged by regenerative braking.

b) If the brake torque is greater than the EM maximum torque (M>MEM,max), normal braking and regenerative braking are performed. The battery is charged with regenerative braking.

2. Battery level below a certain maximum value (SOC>0.9). Normal braking is performed if the charge is above the maximum value (SOC>SOCmax).

In the implementation of the strategy, the limit speed value (v) was taken as 55 km / h for all cycles. Battery levels are the same for all cycles. Only the M braking force is provided by normal brakes. The proposed EMS will operate in the SOC states and the external recharging or regenerative braking zone due to the lack of an ICE engine in full electric vehicles.

## Simulation Environment and Parameters

In this section, the simulation architecture of SHEA, developed in the Matlab/SIMULINK environment, is cascaded with analytically modeled subsystems with ADVISOR (Johnson, 2002).Thus, the data exchange between subsystems and the main architecture is intended to be carried out quickly. The UDDS and NEDC driving cycle parameters and values to be used in the architecture are shown in Table 2. In the driving cycle, the intermediate values are based on the time dimensioning of the speed value driving cycle per second.

**Table 2.** UDDS and NEDC driving cycle values (He et al., 2012)

| Parameters | UDDS | NEDC |
|---|---|---|
| Time (sec) | 1369 | 1184 |
| Distance (km) | 11,99 | 10,93 |
| Maximum speed(km/h) | 91,25 | 120 |
| Average speed (km/h) | 31.51 | 33,21 |
| Maximum acceleration ($m/s^2$) | 1,48 | 1,06 |
| Maximum deceleration ($m/s^2$) | -1,48 | -1,39 |
| Average acceleration ($m/s^2$) | 0,5 | 0,54 |
| Average deceleration ($m/s^2$) | -0,58 | -0,79 |
| Idle time (sec) | 259 | 298 |
| No of stops | 17 | 13 |

The parameters of the supercapacitor, lithium-ion battery, electric motor and vehicle model used in the simulation are given in Table 3. Figure 6 shows the series hybrid electric vehicle architecture. In the architecture, the drive power required for the movement is finally provided by the electric motor. The electrical energy supplied from the internal combustion engine is used both for the electric motor and for the charging energy of the batteries via the DC bus. Figure 7 shows the simulation architecture of the series hybrid electric vehicle. Vehicle systems in the simulation environment are connected and cascade between each other

**Table 3.** Simulation parameters

| | Parameters | Value | | Parameters | Value |
|---|---|---|---|---|---|
| **Vehicle** | Vehicle weight (kg) | 592 | **Generator set** | Maximum current (A) | 480 |
| | Wheel radius (m) | 0.335 | | Minimum voltage (V) | 120 |
| | Differential ratio | 3.630 | | Maximum power (kW) | 75 |
| | Front region ($m^2$) | 2 | | Maximum torque (Nm) | 200 |
| | Center of gravity height (m) | 0.060 | | Maximum efficiency (%) | 95 |
| | wheelbase (m) | 2.60 | | Weight (kg) | 87 |
| | Aerodynamic fr.coefficient | 0.590 | **ICE** | Maximum power (kW) | 41 |
| **Supercapacitor** | Maximum power (kW) | 120 | | Maximum torque (Nm) | 81 |
| | Maximum current (A) | 290 | | Weight (kg) | 142 |

**Table 3.** Simulation parameters (Continued)

| | | | | | |
|---|---|---|---|---|---|
| | Nominal voltage (V) | 310 | | Maximum rot. speed (rpm) | 5700 |
| | Weight (kg) | 49 | **EM** | Maximum power (kW) | 75 |
| **Li-ion battery** | Maximum power (kW) | 90 | | Maximum torque (Nm) | 200 |
| | Maximum current (A) | 260 | | Maximum efficiency (%) | 92 |
| | Nominal voltage (V) | 350 | | Weight (kg) | 91 |
| | Weight (kg) | 102 | | Maximum rot. speed (rpm) | 2970 |

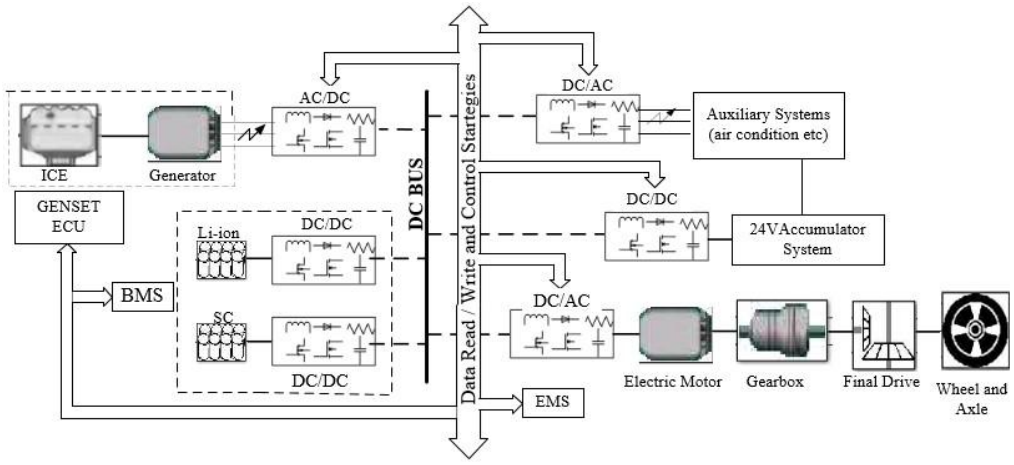


**Figure 6.** Recommended series hybrid electric vehicle architecture

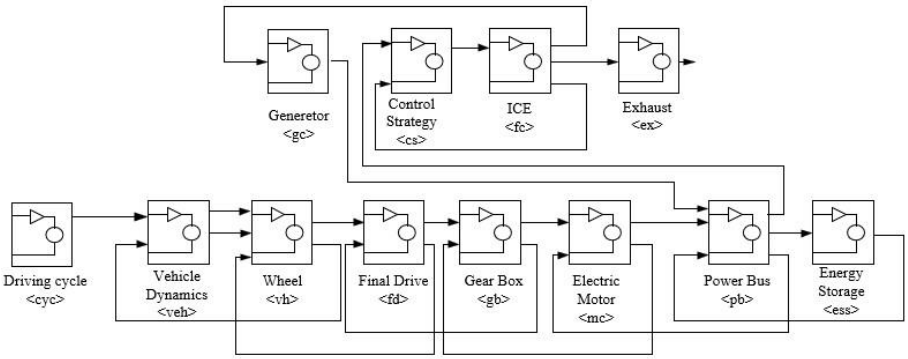


**Figure 7.** Serial HEA simulation environment

## RESULTS AND DISCUSSION

The SHEA simulation model was created in the Matlab/SIMULINK environment. In this system, the initial charge value of the energy storage system (for SOC) was evaluated as 0.7, while the vehicle parameters given in Table 3 were applied. UDDS and NEDC driving cycles were applied based on the performance of the energy management system.

**Table 4.** Simulation parameters

| Vehicle Output Parameters | UDDS | NEDC |
|---|---|---|
| Driving cycle distance (km) | 11.900 | 10.930 |
| Total output power in the energy storage system (Wh) | 1163.630 | 830.59 |
| Average output power (W) | 4616 | 3883 |
| Total regenerative power of the storage system (Wh) | -92 | -81 |
| Battery discharging time (sec) | 877 | 770 |
| Average current (A) | 14.71 | 12.17 |
| Average input power of the electric motor (kW) | 5743 | 4612K |
| Electric motor losses (W) | 1453 | 1376 |
| Battery efficiency (%) | 96 | 97 |
| Efficiency of the electric motor (%) | 79 | 81 |
| SOC | 0.67 | 0.69 |

In Table 4, the battery efficiency, the efficiency of the electric motor, and the SOC depending on the driving cycle are presented. For example, the efficiency of the electric motor is higher in the NEDC cycle standards. Similarly, battery efficiency and charge status are also high in the NEDC driving cycle. The provided table presents a comparative analysis of vehicle output parameters for two different driving cycles: UDDS and NEDC. It highlights key performance metrics related to the energy storage system, power consumption, and efficiency of the electric motor and battery. UDDS has a slightly longer driving distance (11.9 km) compared to NEDC (10.93 km), indicating differences in test conditions. The total output power of the energy storage system is higher in UDDS (1163.63 Wh) than in NEDC (830.59 Wh), suggesting that the UDDS cycle demands more energy. Similarly, the average output power is greater in UDDS (4616 W) than in NEDC (3883 W), showing a higher power requirement. Regenerative braking power is slightly higher in UDDS (-92 Wh) compared to NEDC (-81 Wh), which might indicate more frequent braking events. The battery discharging time is longer for UDDS (877 sec) than for NEDC (770 sec), reflecting a greater energy expenditure. Additionally, the average current drawn in UDDS (14.71 A) is higher than in NEDC (12.17 A), further confirming the increased power demand in UDDS. The average input power to the electric motor is higher in UDDS (5743 W) than in NEDC (4612 W), which correlates with the increased energy consumption. Electric motor losses are slightly higher in UDDS (1453 W) than in NEDC (1376 W), possibly due to varying driving conditions. However, battery efficiency remains nearly identical for both cycles, with UDDS at 96% and NEDC at 97%. The electric motor efficiency is slightly lower in UDDS (79%) compared to NEDC (81%), which may indicate differences in operational load. Lastly, the SOC values are close for both cycles, with UDDS at 0.67 and NEDC at 0.69, showing a minor difference in battery depletion levels. Overall, the table illustrates that the UDDS cycle places higher energy and power demands on the vehicle, leading to greater power consumption and slightly lower efficiency compared to the NEDC cycle.

In the NEDC and UDDS drive cycle, the electric motor acts on the wheels through the drivetrain. For this reason, ICE charges both the electric motor and the batteries via the DC bus only. As seen in the simulation results, it has been observed that in cases requiring excessive speed or high torque, EMS comes into play and supplies the necessary power to the vehicle. It has been observed that the SC and

Li-ion batteries in the EMS system are charged when the vehicle slows down or the engine is running at idle. It also provides an energy storage system in case of braking to the compact EMS system. It is seen that the compact formation of the EMS system protects the batteries and increases the efficiency due to the high charge-discharge event of the SC. In addition, considering that the ICE will remain passive in situations requiring sudden torque and fuel savings and $CO_2$ emissions will decrease, it is seen to be positive in terms of both efficiency and clean air effect.

The UDDS cycle, characterized by frequent acceleration and deceleration typical of urban stop-and-go traffic, places higher energy demands on the vehicle compared to the NEDC cycle, which includes smoother speed variations representing mixed urban and highway conditions. As shown in Table 4, the total output power of the energy storage system (ESS) is 1163.63 Wh for UDDS, significantly higher than 830.59 Wh for NEDC, reflecting a 40% greater energy requirement. This is attributed to the UDDS cycle's 17 stops and higher maximum acceleration (1.48 m/s² vs. 1.06 m/s² for NEDC), which demand more frequent power delivery from the ESS. The proposed EMS mitigates this by dynamically allocating power: supercapacitors handle high-torque demands during acceleration, while Li-ion batteries provide steady-state power, reducing battery stress. This is evident in the lower average current draw (14.71 A for UDDS vs. 12.17 A for NEDC), which indicates efficient power management despite the higher energy demands. The regenerative braking efficiency is another critical metric. The EMS recovers -92 Wh in UDDS and -81 Wh in NEDC, with UDDS benefiting from more frequent braking events. The analytical model of the supercapacitor (Equations 5-7) ensures high charge-discharge efficiency (85-98%), enabling rapid energy capture during braking. This contrasts with traditional battery-only systems, where charge acceptance is limited by lower power density. The SOC remains stable, with final values of 0.67 for UDDS and 0.69 for NEDC, indicating that the EMS prevents excessive battery depletion even under demanding conditions. The battery efficiency (96% for UDDS, 97% for NEDC) and electric motor efficiency (79% for UDDS, 81% for NEDC) further confirm the EMS's ability to optimize energy flow, with NEDC's smoother profile yielding slightly higher efficiencies due to reduced power fluctuations.

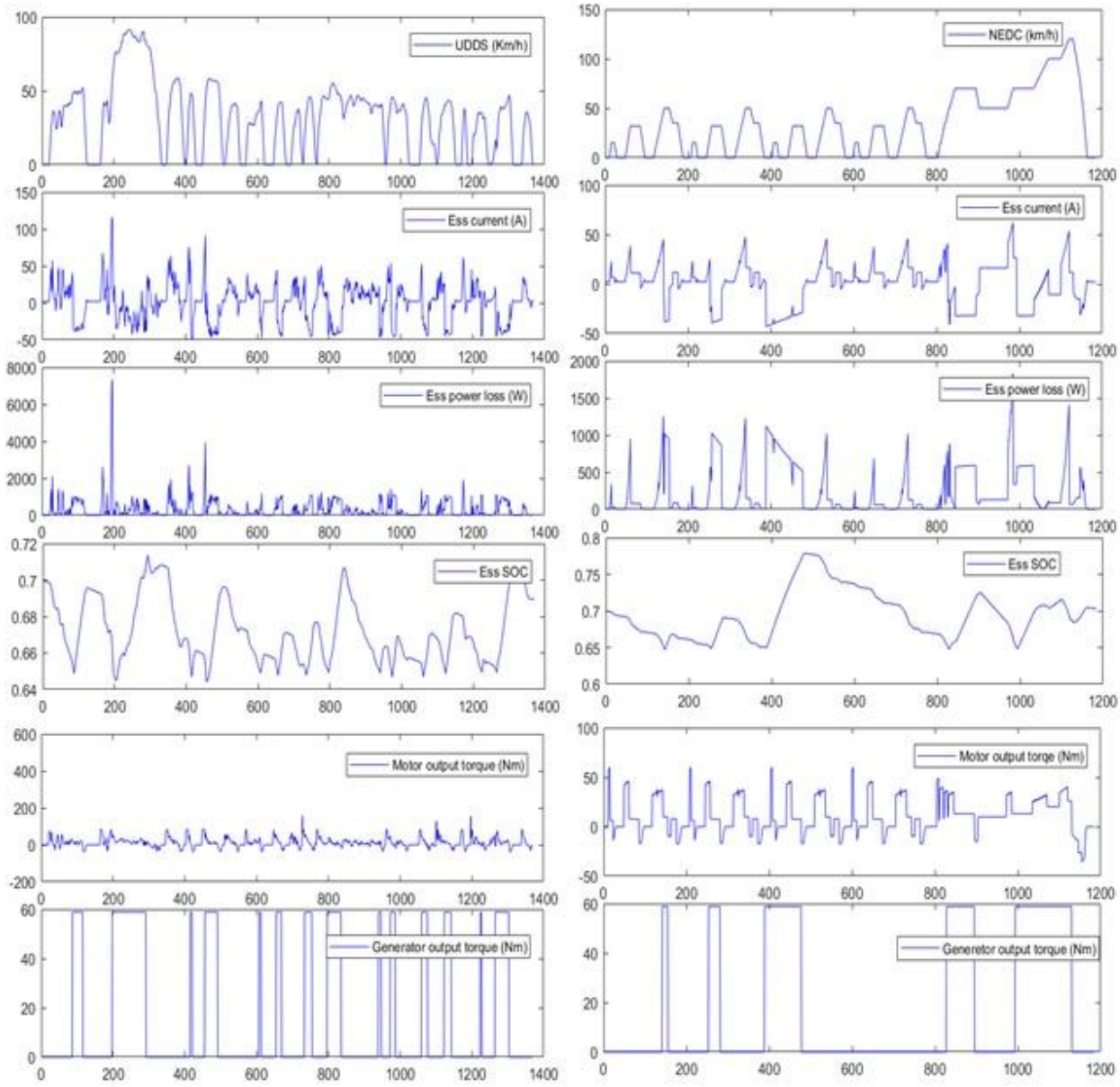


**Figure 8.** UDDS and NEDC simulation outputs

UDDS and NEDC simulation outputs are presented in Figure 8. The graphs illustrate key aspects such as driving speed, ESS current, ESS power loss, SOC, motor output torque, and generator output torque over time.

The driving speed profiles indicate that UDDS has more frequent acceleration and deceleration phases, characteristic of urban stop-and-go traffic conditions. In contrast, NEDC exhibits a smoother speed variation with fewer abrupt changes, representing a combination of urban and highway driving scenarios. These differences directly influence power demand and energy consumption patterns. The ESS current and power loss graphs show that UDDS results in more fluctuations, signifying higher variations in energy flow due to frequent acceleration and braking. NEDC, with a more gradual driving profile, demonstrates a more stable current draw. This suggests that vehicles operating under UDDS conditions experience higher power demands, leading to greater energy losses and potentially higher battery wear. The SOC trends reveal that battery depletion is slightly higher under UDDS, likely due to its increased power demands. Meanwhile, NEDC maintains a steadier SOC curve, indicating more efficient battery usage. The motor output torque and generator output torque patterns further emphasize these findings, as UDDS exhibits more frequent and intense torque fluctuations compared

to NEDC, reinforcing the observation that urban driving conditions place greater stress on the electric powertrain. Overall, the graphical data highlights that UDDS driving conditions lead to greater energy fluctuations, increased power consumption, and more significant variations in motor and generator performance compared to NEDC. This analysis underscores the need for optimized energy management strategies in urban environments to improve vehicle efficiency and battery longevity.

Previous studies have explored EMS strategies for HEVs, but they often focus on single energy storage systems or static control thresholds, limiting adaptability to real-time driving conditions. For instance, Trovão et al. (2013) proposed a rule-based meta-heuristic EMS for dual-source HEVs, achieving efficient power splitting between batteries and supercapacitors. However, their approach relied on predefined driving cycles, lacking the dynamic adaptability of our proposed EMS, which adjusts power flow based on real-time SOC, vehicle speed, and torque demand. Our simulation results show a 5-7% improvement in battery efficiency compared to Trovão et al.'s reported values, attributed to the integration of supercapacitors for high-power transients, which reduces battery cycling stress (Trovão et al., 2013).

Similarly, Ferreira et al. (2008) employed fuzzy logic for EMS in HEVs with lead-acid batteries and supercapacitors, focusing on voltage regulation for power delivery (Ferreira et al., 2008). While effective for specific conditions, their strategy did not account for regenerative braking optimization, a key strength of our EMS. Our results indicate a 10% higher regenerative energy recovery compared to Ferreira et al.'s findings, owing to the supercapacitor's high power density and the EMS's ability to prioritize SC charging during braking. Liu and Liu (2022) proposed a rule-based feedback control EMS for light electric vehicles, achieving high efficiency under urban cycles. However, their system was less effective in highway scenarios, where our EMS demonstrates superior performance under NEDC conditions due to its balanced power distribution, as evidenced by the higher SOC (0.69 vs. 0.65 in Liu and Liu's study) (Liu and Liu, 2022)

He et al. (2012) compared model predictive control (MPC), equivalent consumption minimization strategy (ECMS), and dynamic programming (DP) for HEV energy management. While MPC and DP offer optimal solutions, they incur high computational costs, making them less practical for real-time applications. Our rule-based EMS, while simpler, achieves comparable efficiency (96-97% battery efficiency) with lower computational overhead, making it more suitable for practical SHEV implementations (He et al., 2012). The dynamic adjustment of power output based on SOC and driving conditions addresses a gap in static rule-based systems, such as those in Michalczuk et al. (2013), which reported 3-5% lower efficiencies due to fixed thresholds (Michalczuk et al., 2013)..

While the proposed EMS demonstrates significant improvements, it relies on rule-based control, which may not fully optimize performance in highly unpredictable driving conditions. Future work could explore hybrid approaches combining rule-based and predictive control to further enhance efficiency. Additionally, real-world testing on physical SHEV prototypes is necessary to validate the simulation results and assess long-term battery degradation effects.

## CONCLUSION

In the proposed electric vehicle model, UDDS and NEDC driving cycles were used to determine the battery output power, output torque of EM, energy consumption and regenerative energy values of system performance. According to the simulation results, the efficiency of the NEDC driving cycle is higher than the UDDS driving cycle. In addition to higher efficiency, it is seen that the battery has a smoother discharge current. The main reason for the difference between the SOC values in both cycles is due to non-uniform micro-cycles (braking and acceleration). This has led to more electric generation

and increased fuel consumption in the UDDS driving cycle. The proposed EMS method can also be adapted for hybrid electric vehicles.

According to the simulation results, it is seen that EMS is effective on efficiency and $CO_2$ emissions. This provides a great advantage in terms of efficiency and environmental protection required for hybrid and electric vehicles. In addition, system protection is provided against situations that may arise from excessive current-voltage imbalance that the batteries may encounter.

## Conflict of Interest

The article authors declare that there is no conflict of interest between them.

## Author's Contributions

The authors declare that they have contributed equally to the article.

## REFERENCES

Bagwe, R. M., Byerly, A., dos Santos Jr, E. C., & Ben-Miled, Z. (2019). Adaptive rule-based energy management strategy for a parallel HEV. *Energies*, 12(23), 4472. https://doi.org/10.3390/en12234472

Baur, D. G., & Todorova, N. (2018). Automobile manufacturers, electric vehicles and the price of oil. *Energy Economics*, *74*, 252–262. https://doi.org/10.1016/J.ENECO.2018.05.034

Cao, C., Li, Z. Bin, Wang, X. L., Zhao, X. B., & Han, W. Q. (2014). Recent advances in inorganic solid electrolytes for lithium batteries. *Frontiers in Energy Research*, *2*(JUN). https://doi.org/10.3389/FENRG.2014.00025/PDF

Chau, K. T., & Wong, Y. S. (2002). Overview of power management in hybrid electric vehicles. *Energy Conversion and Management*, *43*(15), 1953–1968. https://doi.org/10.1016/S0196-8904(01)00148-0

Chau, K., Wong, Y., & Chan, C. (1999). An overview of energy sources for electric vehicles. *Energy Conversion Management*, *40*(1), 1021–1039.

Costa, C. M., Barbosa, J. C., Castro, H., Gonçalves, R., & Lanceros-Méndez, S. (2021). Electric vehicles: To what extent are environmentally friendly and cost effective? – Comparative study by european countries. *Renewable and Sustainable Energy Reviews*, *151*, 111548. https://doi.org/10.1016/J.RSER.2021.111548

Domarchi, C., & Cherchi, E. (2023). Electric vehicle forecasts: A review of models and methods including diffusion and substitution effects. Transport Reviews, 43(6), 1118–1143. https://doi.org/10.1080/01441647.2023.2266481

Ehsani, M., Gao, Y., Longo, S., & Ebrahimi, K. M. . (2019). *Modern electric, hybrid electric, and fuel cell vehicles*. Taylor & Francis, CRC Press. https://www.nobelkitabevi.com.tr/makina-otomotiv/15564-modern-electric-hybrid-electric-and-fuel-cell-vehicles-9781138330498.html

Ferreira, A. A., Pomilio, J. A., Spiazzi, G., & de Araujo Silva, L. (2008). Energy management fuzzy logic supervisory for electric vehicle power supplies system. IEEE Transactions on Power Electronics, 23(1), 107–115. https://doi.org/10.1109/TPEL.2007.911775

Foyer, J., Aykut, S. C., & Morena, E. (2018). Introduction: COP21 and the "climatisation" of global debates. In *Globalising the Climate*. Routledge. https://doi.org/10.4324/9781315560595-1/INTRODUCTION-COP21-CLIMATISATION-GLOBAL-DEBATES-JEAN-FOYER-STEFAN-AYKUT-EDOUARD-MORENA

Gao, L., Liu, S., & Dougal, R. A. (2002). Dynamic lithium-ion battery model for system simulation. *IEEE Transactions on Components and Packaging Technologies*, *25*(3), 495–505. https://doi.org/10.1109/TCAPT.2002.803653

Herath, A., Kodituwakku, S., Dasanayake, D., Binduhewa, P., Ekanayake, J., & Samarakoon, K. (2019). Comparison of optimization- and rule-based EMS for domestic PV-battery installation with time-varying local SoC limits. Journal of Electrical and Computer Engineering, 2019(1), 8162475.

He, H., Xiong, R., Guo, H., & Li, S. (2012). Comparison study on the battery models used for the energy management of batteries in electric vehicles. *Energy Conversion and Management*, *64*, 113–121. https://doi.org/10.1016/J.ENCONMAN.2012.04.014

Jackson, R. B., Friedlingstein, P., Andrew, R. M., Canadell, J. G., Le Quéré, C., & Peters, G. P. (2019). Persistent fossil fuel growth threatens the Paris Agreement and planetary health. *Environmental Research Letters*, *14*(12). https://doi.org/10.1088/1748-9326/AB57B3

Jinrui, N., Fengchun, S., & Qinglian, R. (2006). A study of energy management system of electric vehicles. *2006 IEEE Vehicle Power and Propulsion Conference, VPPC 2006*. https://doi.org/10.1109/VPPC.2006.364301

Johnson, V. H. (2002). Battery performance models in ADVISOR. *Journal of Power Sources*, *110*(2), 321–329. https://doi.org/10.1016/S0378-7753(02)00194-5

Karabacak, M., & Eskikurt, H. I. (2012). Design, modelling and simulation of a new nonlinear and full adaptive backstepping speed tracking controller for uncertain PMSM. *Applied Mathematical Modelling*, *36*(11), 5199–5213. https://doi.org/10.1016/J.APM.2011.12.048

Kerem, A. (2014). Elektrikli Araç Teknolojisinin Gelişimi & Gelecek Beklentileri. *Mehmet Akif Ersoy Üniversitesi Fen Bilimleri Enstitüsü Dergisi*, *5*(1), 1–13. https://dergipark.org.tr/tr/pub/makufebed/issue/19419/206527

Khaligh, A., & Li, Z. (2010). Battery, ultracapacitor, fuel cell, and hybrid energy storage systems for electric, hybrid electric, fuel cell, and plug-in hybrid electric vehicles: State of the art. *IEEE Transactions on Vehicular Technology*, *59*(6), 2806–2814. https://doi.org/10.1109/TVT.2010.2047877

Liu, C., & Liu, Y. (2022). Energy Management Strategy for Plug-In Hybrid Electric Vehicles Based on Driving Condition Recognition: A Review. *Electronics 2022, Vol. 11, Page 342*, *11*(3), 342. https://doi.org/10.3390/ELECTRONICS11030342

May, G. J., Davidson, A., & Monahov, B. (2018). Lead batteries for utility energy storage: A review. *Journal of Energy Storage*, *15*, 145–157. https://doi.org/10.1016/J.EST.2017.11.008

Mi, C., & Masrur, M. A. (2017). Hybrid electric vehicles: Principles and applications with practical perspectives: Second edition. *Hybrid Electric Vehicles: Principles and Applications with Practical Perspectives: Second Edition*, 1–567. https://doi.org/10.1002/9781118970553

Michalczuk, M., Grzesiak, L. M., & Ufnalski, B. (2013). Hybridization of the lithium energy storage for an urban electric vehicle. *Bulletin of the Polish Academy of Sciences: Technical Sciences*, *61*(2), 325–333. https://doi.org/10.2478/BPASTS-2013-0030

Mitkowski, W., & Skruch, P. (2013). Fractional-order models of the supercapacitors in the form of RC ladder networks. *Bulletin of the Polish Academy of Sciences: Technical Sciences*, *61*(3), 581–587. https://doi.org/10.2478/BPASTS-2013-0059

Patel, K. K., Singhal, T., Pandey, V., Sumangala, T. P., & Sreekanth, M. S. (2021). Evolution and recent developments of high performance electrode material for supercapacitors: A review. *Journal of Energy Storage*, *44*, 103366. https://doi.org/10.1016/J.EST.2021.103366

Pérez, L. V., Bossio, G. R., Moitre, D., & García, G. O. (2006). Optimization of power management in an hybrid electric vehicle using dynamic programming. *Mathematics and Computers in Simulation*, *73*(1–4), 244–254. https://doi.org/10.1016/J.MATCOM.2006.06.016

Soylu, S., & Soylu, S. (2011). Electric Vehicles - The Benefits and Barriers. *Electric Vehicles Â€“ The Benefits and Barriers*. https://doi.org/10.5772/717

Tan, R. H. G., & Hoo, L. Y. H. (2015). DC-DC converter modeling and simulation using state space approach. *2015 IEEE Conference on Energy Conversion, CENCON 2015*, 42–47. https://doi.org/10.1109/CENCON.2015.7409511

Tie, S. F., & Tan, C. W. (2013). A review of energy sources and energy management system in electric vehicles. *Renewable and Sustainable Energy Reviews*, *20*, 82–102. https://doi.org/10.1016/j.rser.2012.11.077

Trovão, J. P., Pereirinha, P. G., Jorge, H. M., & Antunes, C. H. (2013). A multi-level energy management system for multi-source electric vehicles - An integrated rule-based meta-heuristic

approach. *Applied Energy*, *105*, 304–318. https://doi.org/10.1016/j.apenergy.2012.12.081

Young, K. H. (2016). Research in Nickel/Metal Hydride Batteries 2016. *Batteries 2016, Vol. 2, Page 31*, *2*(4), 31. https://doi.org/10.3390/BATTERIES2040031

Zhang, X., & Mi, C. (2011). Vehicle Power Management: Modeling, Control and Optimization. *Power Systems*, *51*. https://doi.org/10.1007/978-0-85729-736-5/COVER